JOURNAL OF SPACECRAFT AND ROCKETS
Vol. 44, No. 4, July–August 2007

Impact of Optical Degradation on Solar Sail Mission Performance

Bernd Dachwald*
DLR, German Aerospace Center, 51147 Cologne, Germany
Malcolm Macdonald†
University of Glasgow, Glasgow, G12 8QQ Scotland, United Kingdom
Colin R. McInnes‡
University of Strathclyde, Glasgow, G1 1XJ Scotland, United Kingdom
and
Giovanni Mengali§ and Alessandro A. Quarta¶
University of Pisa, 56122 Pisa, Italy

DOI: 10.2514/1.21432

The optical properties of the thin metalized polymer films that are projected for solar sails are likely to be affected by the damaging effects of the space environment, but their real degradation behavior is to a great extent unknown. The standard solar sail force models that are currently used for solar sail mission analysis and design do not take these effects into account. In this paper we use a parametric model to describe the sail film's optical degradation with its environmental history to estimate the impact of different degradation behaviors on solar sail mission performance for some example interplanetary missions: Mercury rendezvous missions, fast missions to Neptune and to the heliopause, and artificial Lagrange-point missions.

Nomenclature

A	=	sail area
$\boldsymbol{a}$	=	acceleration vector
a_c	=	characteristic acceleration
a_1, a_2, a_3	=	force coefficients
B	=	non-Lambertian coefficient
c	=	speed of light in vacuum
d	=	degradation factor
$\boldsymbol{e}_r, \boldsymbol{e}_t, \boldsymbol{e}_h$	=	unit vectors of the orbital reference frame
$\boldsymbol{e}_x, \boldsymbol{e}_y, \boldsymbol{e}_z$	=	unit vectors of the inertial reference frame
$\boldsymbol{F}$	=	force vector
$\mathcal{I}$	=	inertial reference frame
m	=	sailcraft mass
$\boldsymbol{m}$	=	thrust unit vector
$\boldsymbol{n}$	=	sail normal (unit) vector
$\mathcal{O}$	=	orbital reference frame
P	=	solar radiation pressure
$\mathcal{P}$	=	set of optical coefficients
p	=	arbitrary optical coefficient $\in \mathcal{P}$
$\boldsymbol{r}$	=	position vector ($r \triangleq \|\boldsymbol{r}\|$)
r_0	=	1 astronomical unit, 1 AU
S	=	solar radiation flux
$\mathcal{S}$	=	sail-fixed reference frame
S_0	=	solar constant
s	=	specular reflection factor
T	=	sail equilibrium temperature
t	=	time
$\boldsymbol{t}$	=	sail tangential (unit) vector
U	=	three-body gravitational potential
$\boldsymbol{u}$	=	control vector
$\boldsymbol{v}$	=	velocity vector
$\boldsymbol{x}$	=	state vector
α	=	sail pitch angle
β	=	lightness number
δ	=	sail clock angle
ε	=	emission coefficient
η	=	reflection coefficient (model SNPR)
θ	=	sail cone angle
λ	=	degradation constant
μ	=	sun's gravitational parameter
ρ	=	reflection coefficient (model NPR)
Σ	=	dimensionless solar radiation dose
$\tilde{\Sigma}$	=	solar radiation dose
$\hat{\Sigma}$	=	half-life solar radiation dose
σ	=	sail loading
ϕ	=	centerline angle
Ψ	=	force function [see Eq. (5)]
$\boldsymbol{\omega}$	=	angular velocity of the two primary masses in the three-body problem

Subscripts

b	=	sail backside
f	=	final
fr	=	sail front side
lim	=	limit
max	=	maximum
SRP	=	solar radiation pressure
0	=	initial; reference; at 1 AU
1	=	primary body in the three-body problem
2	=	secondary body in the three-body problem
$\parallel$	=	sail tangential
$\perp$	=	sail normal
∞	=	end of life

Superscript

$\dot{}$	=	time derivative

Received 28 November 2005; revision received 15 August 2006; accepted for publication 18 December 2006.

*Scientist, Current Address: DLR, German Aerospace Center, Mission Operations Section, 82230 Oberpfaffenhofen, Germany; bernd.dachwald@dlr.de. Member AIAA.

†Research Assistant, Current Address: SciSys, Bristol, BS4 5SS England, United Kingdom; malcolm.macdonald@scisys.co.uk.

‡Professor, Department of Mechanical Engineering; colin.mcinnes@strath.ac.uk. Member AIAA.

§Associate Professor, Department of Aerospace Engineering; g.mengali@ing.unipi.it. Member AIAA.

¶Research Assistant, Department of Aerospace Engineering; a.quarta@ing.unipi.it. Member AIAA.

Introduction

SOLAR sail technology has been identified as enabling for many recent space mission concepts due to its capability of reducing the mission costs and increasing the payload mass fraction. Moreover, the continuous advances in material technology can enable near-term solar sail missions that would be prohibitive for other types of primary propulsion [1]. A realistic mission analysis, however, is a demanding task because solar sail performance is significantly affected by both the sail geometry [2] and the optical properties of the sail film [3].

The nonperfectly reflecting solar sail model according to [4] (referred to as model NPR), and also described in [5,6], is widely used for solar sail mission analysis, even if most of the currently available results have been obtained using an even simpler model with ideal reflection (model IR). Based on model NPR, Rios-Reyes and Scheeres [7] recently proposed a generalized sail model (GSM) for nonflat solar sails, which allows one to take into account also the local variation effects of the optical sail properties. Nevertheless, all the preceding models are still quite unsatisfactory because the optical properties of the thin metalized solar sail polymer films are assumed to be not degraded by the space environment but to be constant.

In contrast, the fundamental assumption of this paper is that the optical properties of solar sail films *are* degraded by the harsh space environment. Although significant ground and space testing has been performed to measure the optical degradation of metalized polymer films as second surface mirrors (metalized on the back side), to our knowledge, no *systematic* testing to measure the optical degradation of candidate solar sail films (metalized on the front side) has been reported so far. Lura et al. [8] pointed out the considerable effects caused by a combined irradiation with vacuum ultraviolet (VUV) radiation, electrons, and protons, whereas Edwards et al. [9] emphasized that a change of the solar absorption and emission coefficients cannot be measured after irradiation with electrons alone. Because a corresponding in-space testing campaign has not yet been done, the optical degradation behavior of solar sails, and therefore the degradation behavior of their propulsive capability in the real space environment is, to a great extent, still unknown.

In [10], some of the authors of this paper have proposed a more realistic parametric model for optical solar sail degradation (OSSD) and have derived the corresponding optimal control laws. This model, which is based on model NPR, describes the variation of the sail film's optical coefficients with time, through a dependence on the sail film's environmental history, that is, the radiation dose. The primary intention of this model is not that of describing the exact behavior of specific film-coating combinations in the real space environment, but rather that of providing a flexible parametric framework for representing the general optical degradation behavior of solar sails. This model is, of course, susceptible to further refinements, especially when the results obtained from both ground and in-space tests would become available. Until then, it can be used to investigate the impact of different potential degradation behaviors on various mission aspects by simply varying the OSSD model parameters, as is done within this paper.

This paper is organized as follows. First, the solar radiation pressure (SRP) force model for nonperfectly reflecting solar sails with optical degradation is briefly revisited for convenience. This model is then used to estimate the impact of OSSD on mission performance for several example interplanetary missions: Mercury rendezvous missions, fast missions to Neptune and to the heliopause, and artificial Lagrange-point missions.

Nonperfectly Reflecting Solar Sail with Optical Degradation

For the description of the SRP force exerted on a solar sail, $\boldsymbol{F}_{\mathrm{SRP}}$, it is useful to introduce two unit vectors. The first one is $\boldsymbol{n}$, which is perpendicular to the sail surface and always directed away from the sun. The second one is $\boldsymbol{m}$, which points along the direction of $\boldsymbol{F}_{\mathrm{SRP}}$. Let $\mathcal{O} = \{\boldsymbol{e}_r, \boldsymbol{e}_t, \boldsymbol{e}_h\}$ be an orthogonal right-handed Cartesian coordinate frame, where $\boldsymbol{e}_r$ points along the sun-spacecraft line, $\boldsymbol{e}_h$ is normal to the orbit plane (pointing along the spacecraft's orbital angular momentum vector), and $\boldsymbol{e}_t$ completes the right-handed coordinate system. In $\mathcal{O}$, the direction of $\boldsymbol{n}$, which describes the sail attitude, is expressed through the pitch angle α and the clock angle δ, while the direction of $\boldsymbol{m}$ is described by the cone angle θ and the clock angle δ (see Fig. 1).

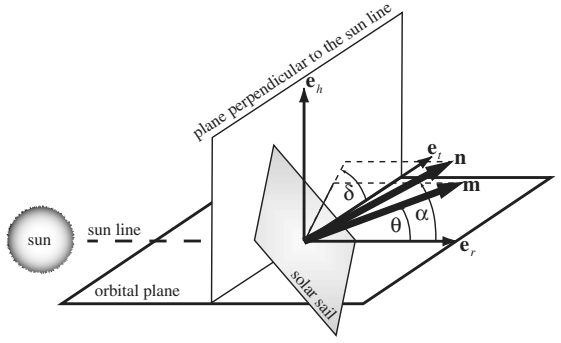

Fig. 1 Definition of the sail normal vector and the thrust normal vector.

The OSSD model is based on the model in [4], model NPR, which parametrizes the optical characteristics of the real sail film through a set of optical coefficients $\mathcal{P} = \{\rho, s, \varepsilon_{\mathrm{fr}}, \varepsilon_b, B_{\mathrm{fr}}, B_b\}$ (ρ is the reflection coefficient, s is the specular reflection factor, $\varepsilon_{\mathrm{fr}}$ and ε_b are the emission coefficients of the front and back sides, respectively, and B_{fr} and B_b are the non-Lambertian coefficients of the front and back sides, respectively). The optical coefficients for a solar sail with a highly reflective aluminum-coated front side and with a highly emissive chromium-coated back side (to keep the sail temperature at a moderate limit) are $\mathcal{P}_{\mathrm{Al|Cr}} = \{\rho = 0.88, s = 0.94, \varepsilon_{\mathrm{fr}} = 0.05, \varepsilon_b = 0.55, B_{\mathrm{fr}} = 0.79, B_b = 0.55\}$ [4].

At a distance r from the sun, the SRP is

$$P = \frac{S_0}{c}\left(\frac{r_0}{r}\right)^2 = P_0 \cdot \left(\frac{r_0}{r}\right)^2 = 4.563\ \frac{\mu\mathrm{N}}{\mathrm{m}^2} \cdot \left(\frac{r_0}{r}\right)^2 \tag{1}$$

where $S_0 = 1368\ \mathrm{W/m^2}$ is the solar constant. The SRP force exerted on a solar sail of area A can be decomposed in a sail-fixed two-dimensional coordinate frame $\mathcal{S} = \{\boldsymbol{n}, \boldsymbol{t}\}$ (because of symmetry, the third dimension is not relevant here) through a normal component $F_\perp$ along $\boldsymbol{n}$ and a tangential component $F_\parallel$ along $\boldsymbol{t}$ (see Fig. 2), where

$$F_\perp = \boldsymbol{F}_{\mathrm{SRP}} \cdot \boldsymbol{n} = 2PA\cos\alpha(a_1\cos\alpha + a_2) \tag{2a}$$

$$F_\parallel = \boldsymbol{F}_{\mathrm{SRP}} \cdot \boldsymbol{t} = -2PA\cos\alpha a_3 \sin\alpha \tag{2b}$$

with

$$a_1 \triangleq \tfrac{1}{2}(1 + s\rho) \tag{3a}$$

$$a_2 \triangleq \frac{1}{2}\left[B_{\mathrm{fr}}(1-s)\rho + (1-\rho)\frac{\varepsilon_{\mathrm{fr}}B_{\mathrm{fr}} - \varepsilon_b B_b}{\varepsilon_{\mathrm{fr}} + \varepsilon_b}\right] \tag{3b}$$

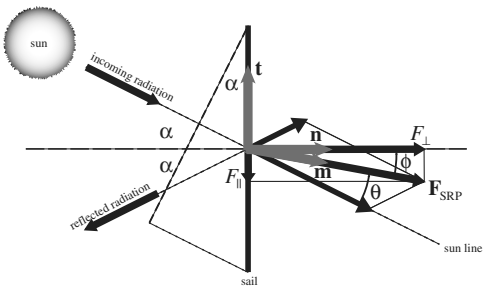

Fig. 2 SRP force on a nonperfectly reflecting sail.

$$a_3 \triangleq \tfrac{1}{2}(1 - s\rho) \tag{3c}$$

The total SRP force can then be written as

$$\boldsymbol{F}_{\mathrm{SRP}} = 2PA\cos\alpha\,\Psi\boldsymbol{m} \tag{4}$$

with

$$\Psi \triangleq [(a_1\cos\alpha + a_2)^2 + (a_3\sin\alpha)^2]^{1/2} \tag{5}$$

Note that Eq. (4) has a structure similar to the equivalent equation for model IR, $\boldsymbol{F}_{\mathrm{SRP}}^{(\mathrm{IR})} = 2PA\cos\alpha\cos\alpha\boldsymbol{n}$, but now the SRP force is smaller and no more directed along $\boldsymbol{n}$.

The performance of a solar sail is usually quantified by the characteristic acceleration a_c, which is defined as the SRP acceleration acting on a solar sail that is oriented perpendicular to the sun line ($\boldsymbol{n} \equiv \boldsymbol{e}_r$) at 1 AU. For model NPR,

$$a_c = \frac{2P_0A}{m}(a_1 + a_2) \tag{6}$$

The following simplifications are assumed for the OSSD model:

1) The only source of degradation are the solar photons and particles. This simplification is reasonable at least in the inner solar system and far from the planets, where the cosmic radiation, the radiation from the planetary radiation belts, and the reactions with particles of the planetary atmospheres can be neglected.

2) The solar photon and particle fluxes do not depend on time (average sun without solar events).

3) The optical coefficients do not depend on the sail temperature.

4) The optical coefficients do not depend on the light incidence angle.

5) No self-healing effects occur in the sail film.

With OSSD, any optical coefficient $p \in \mathcal{P}$ becomes time dependent. With the above simplifications, $p(t)$ is a function of the solar radiation dose (SRD) accepted by the solar sail within the time interval $t - t_0$:

$$\tilde{\Sigma}(t) \triangleq \int_{t_0}^{t} S\cos\alpha\,\mathrm{d}t' = S_0 r_0^2 \int_{t_0}^{t} \frac{\cos\alpha}{r^2}\,\mathrm{d}t' \tag{7}$$

(by using the symbol $\tilde{\Sigma}$ for the SRD, Σ is preserved for the dimensionless SRD). The SRD per year on a surface that is perpendicular to the sun at 1 AU is $\tilde{\Sigma}_0 = S_0 \cdot 1\ \mathrm{yr} = 15.768\ \mathrm{TJ/m^2}$. Using $\tilde{\Sigma}_0$ as a reference value, the SRD can be defined in a dimensionless form as

$$\Sigma(t) \triangleq \frac{\tilde{\Sigma}(t)}{\tilde{\Sigma}_0} = \left(r_0^2 \int_{t_0}^{t} \frac{\cos\alpha}{r^2}\,\mathrm{d}t'\right) \Big/ 1\ \mathrm{yr} \tag{8}$$

It was shown in [10] that the degradation caused by the solar particles can be included in $\Sigma(t)$ and does not have to be considered separately. $\Sigma(t)$ depends on the solar distance history $r[t]$ and the attitude history $\alpha[t]$ of the solar sail. Note that Eq. (8) can be rearranged in differential form as

$$\dot{\Sigma}(t) = \frac{r_0^2}{1\ \mathrm{yr}}\frac{\cos\alpha}{r^2} \quad \text{with} \quad \Sigma(t_0) = 0 \tag{9}$$

It is assumed that $p(t)$ varies exponentially between $p(t_0) = p_0$ and $\lim_{t\to\infty} p(t) = p_\infty$, that is,

$$p(t) = p_\infty + (p_0 - p_\infty)\cdot e^{-\lambda\Sigma(t)} \tag{10}$$

The degradation constant λ is related to the "half-life solar radiation dose" $\hat{\Sigma}$ [that is, $\Sigma = \hat{\Sigma}$ implies $p = (p_0 + p_\infty)/2$] via

$$\lambda = \ell_n\, 2/\hat{\Sigma} \tag{11}$$

Because 12 free parameters (six p_∞ and six $\hat{\Sigma}_p$ in addition to the six p_0) are hardly manageable in a parametric OSSD analysis, the number of free parameters has been reduced by introducing a degradation factor d and using a single half-life SRD $\hat{\Sigma}$ for all p. Because when time increases the reflectivity of the sail decreases, the sail becomes more dull and the emissivity increases, it is assumed that

$$\rho_\infty = \rho_0/(1 + d) \tag{12a}$$

$$s_\infty = s_0/(1 + d) \tag{12b}$$

$$\varepsilon_{\mathrm{fr}\infty} = (1 + d)\varepsilon_{\mathrm{fr}0} \tag{12c}$$

$$\varepsilon_{b\infty} = \varepsilon_{b0} \tag{12d}$$

$$B_{\mathrm{fr}\infty} = B_{\mathrm{fr}0} \tag{12e}$$

$$B_{b\infty} = B_{b0} \tag{12f}$$

According to [10], ε_b, B_{fr}, and B_b are less important for OSSD, so that it is reasonable to assume them constant. The degradation of the optical parameters can be written in dimensionless form as

$$\frac{p(t)}{p_0} = \begin{cases} (1 + de^{-\lambda\Sigma(t)})/(1 + d) & \text{for } p \in \{\rho, s\} \\ 1 + d(1 - e^{-\lambda\Sigma(t)}) & \text{for } p = \varepsilon_{\mathrm{fr}} \\ 1 & \text{for } p \in \{\varepsilon_b, B_{\mathrm{fr}}, B_b\} \end{cases} \tag{13}$$

Figure 3a shows the variation of those coefficients with Σ for different values of the degradation factor d. Figure 3b shows how the maximum sail temperature $T_{\max}$ also varies with Σ for different solar distances [10].

Simulation Model

Besides the gravitational forces of all celestial bodies and the SRP force, many disturbing forces, as caused, for example, by the solar wind, the finiteness of the solar disk, the reflected light from close celestial bodies, and the aberration of solar radiation (Poynting–Robertson effect), influence the motion of solar sails in space. Furthermore, a real solar sail bends and wrinkles, depending on the actual sailcraft design. In principle, all these effects have to be considered for high-precision trajectory determination.

For mission feasibility analysis, and to isolate the effects of OSSD from the other effects that influence the motion of real solar sails in space, the following simplifications are made:

1) The solar sail is a flat plate.

2) The solar sail is moving under the sole influence of solar gravitation and radiation.

3) The sun is a point mass and a point light source.

4) The solar sail attitude can be changed instantaneously.

Let the reference frame $\mathcal{I} = \{\boldsymbol{e}_x, \boldsymbol{e}_y, \boldsymbol{e}_z\}$ be an inertial right-handed Cartesian coordinate frame. Neglecting the disturbing accelerations according to the simplifications made above, the equations of motion for a solar sail in the $\mathcal{I}$ frame are

$$\dot{\boldsymbol{r}} = \boldsymbol{v} \tag{14a}$$

$$\dot{\boldsymbol{v}} = -\frac{\mu}{r^3}\boldsymbol{r} + \frac{\boldsymbol{F}_{\mathrm{SRP}}}{m} \tag{14b}$$

where $\boldsymbol{r} = (r_x, r_y, r_z)$ is the sailcraft position, $\boldsymbol{v} = (\dot{r}_x, \dot{r}_y, \dot{r}_z) = (v_x, v_y, v_z)$ is the sailcraft velocity, $r = |\boldsymbol{r}|$, and μ is the sun's gravitational parameter.

The trajectory optimization problem is to find the optimal control $\boldsymbol{u}(t) = (\alpha(t), \delta(t))$ (where $t_0 \le t \le t_f$), which minimizes the time

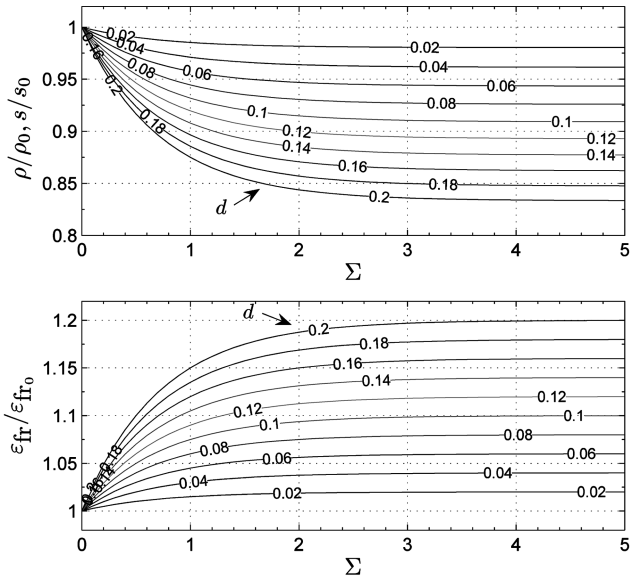

a) Variation of ρ/ρ_0, s/s_0, and $\varepsilon_{fr}/\varepsilon_{fr0}$ with Σ

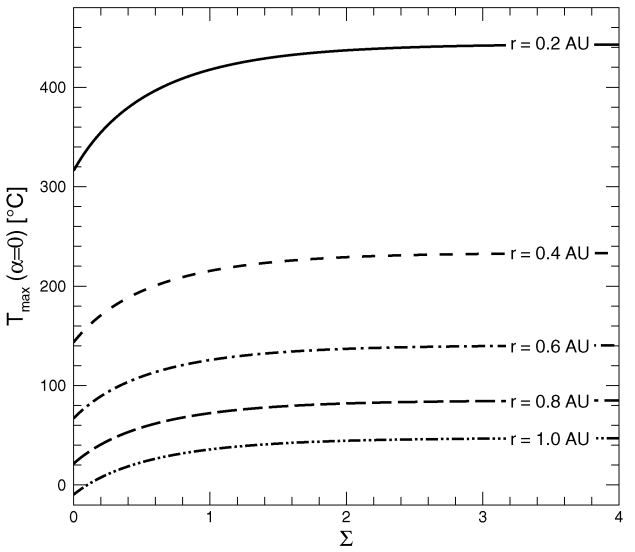

b) Variation of T_{max} with Σ for different solar distances (d=0.2)

Fig. 3 OSSD of the optical parameters and its effect on the sail temperature.

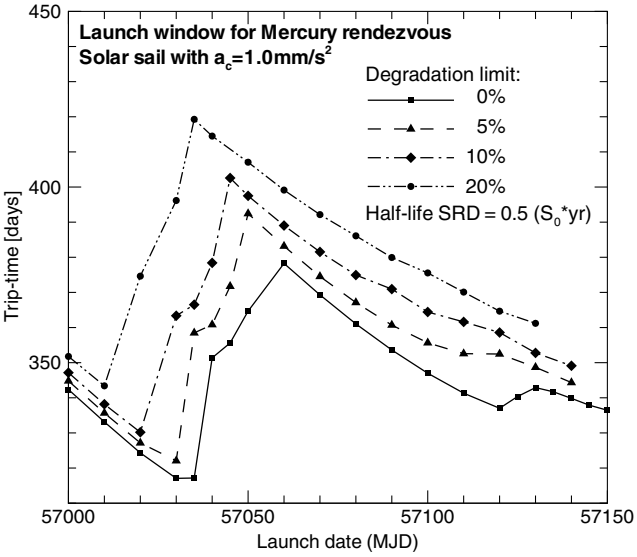

a) Trip-time over launch date

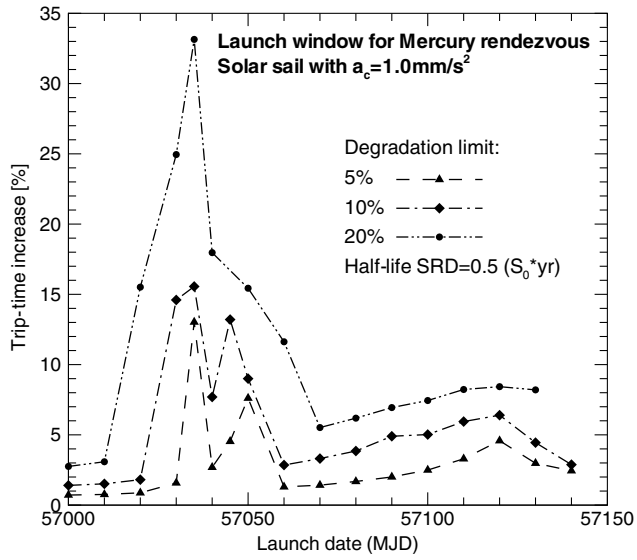

b) Trip-time increase over launch date

Fig. 4 Launch window for Mercury rendezvous for different degradation limits.

$t_f - t_0$ necessary to transfer the spacecraft from an initial state $\boldsymbol{x}_0 = (\boldsymbol{r}_0, \boldsymbol{v}_0)$ to a final state $\boldsymbol{x}_f = (\boldsymbol{r}_f, \boldsymbol{v}_f)$ by maximizing the performance index $J = -(t_f - t_0)$. For an in-depth discussion of the optimal control law, the reader is referred to [10].

Results for Interplanetary Transfer Missions

Mercury Rendezvous Missions

The first case to estimate the impact of OSSD on solar sail mission performance is a Mercury rendezvous using a solar sail with a characteristic acceleration of $a_c = 1.0$ mm/s^2. The trajectories within this section have been calculated using the trajectory optimizer GESOP** with SNOPT [11]. The final accuracy limit for the trajectories was set to a maximum final distance of 80,000 km (lesser than the radius of Mercury's sphere of influence at perihelion) and a maximum final relative velocity of 50 m/s. Trajectories have been calculated for degradation limits of 0, 5, 10, and 20% (to preserve a simple terminology, the term "a 100d% degradation limit" is used synonymously with "a degradation factor of d"), with a half-life SRD of $\hat{\Sigma} = 0.5$ ($S_0 \cdot$ yr). First, the effects of the degradation limit on the trip time was investigated for an arbitrarily selected launch window that ranges from modified Julian date (MJD) 57000 (09 December 2014) to MJD 57130 (18 April 2015). Figure 4a shows the trip time over the launch date, whereas Fig. 4a shows the trip time increase over the launch date. It can be seen from Fig. 4a that the sensitivity of the trip time with respect to OSSD depends considerably on the launch date. Some launch dates that are optimal assuming ideal sail characteristics become very unsuitable when OSSD is taken into account because an additional revolution about the sun is required before rendezvous. Note that the optimal launch date for zero degradation is the worst launch date for a 20% degradation limit. For many launch dates, however, OSSD does not seriously affect the mission, as Fig. 4a shows. Given an indefinite OSSD behavior at launch, MJD 57000.0 would be a very robust launch date. Figure 5a shows the optimal variation of the pitch angle α along the trajectory for this launch date, Fig. 5b for a launch 30 days later. In summary, the results show that OSSD can have remarkable consequences on trip times (Fig. 4) and also on the optimal control angles (Fig. 5). Another important point, which could not be inferred from previously calculated Earth–Mars orbit-to-orbit transfers [10],

**Data available online at http://www.gesop.de [retrieved 31 January 2007].

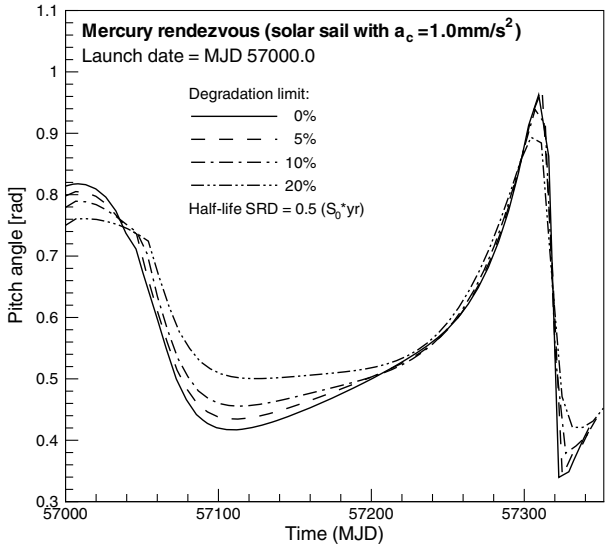

a) Launch at MJD 57000.0

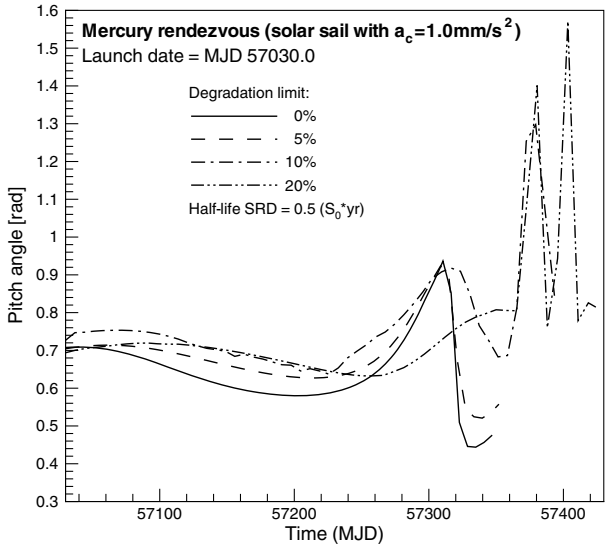

b) Launch at MJD 57030.0

Fig. 5 Optimal sail pitch angle variations for different degradation limits.

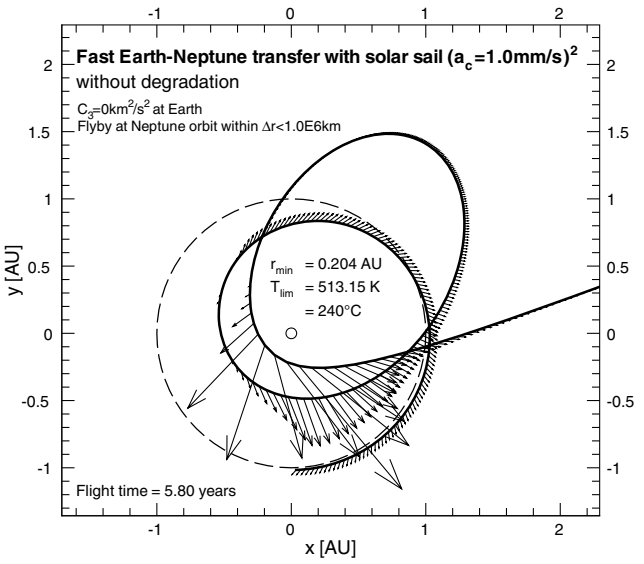

a)

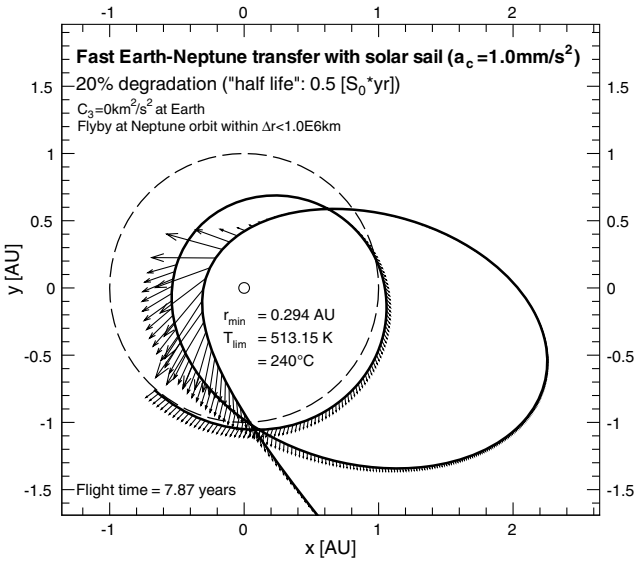

b)

Fig. 6 Topology of optimal Neptune transfer trajectories for different degradation limits.

is that the actual trip time might be tremendously above the lower bound calculated for orbit-to-orbit transfers, if the launch and the target body are in an unfavorable constellation at launch.

Fast Neptune Flyby

The second case to estimate the impact of OSSD on solar sail mission performance is a fast Neptune flyby for a solar sail with a characteristic acceleration of $a_c = 1.0$ mm/s^2. The trajectories within this section have been calculated using InTrance [12], a method that combines artificial neural networks and evolutionary algorithms to find near-globally optimal steering strategies. To find the absolute trip-time minima, independent of the actual constellation of Earth and Neptune, no flyby at Neptune itself, but only a crossing of its orbit within a distance of less than 10^6 km was required, and InTrance was allowed to vary the launch date within a one year interval. Therefore, the resulting trip times represent lower bounds that are strictly valid only for the optimal constellation of Earth and Neptune. Specific suboptimal launch dates/constellations, for example, when Neptune is at aphelion, might yield longer trip times. Although a final distance of 10^6 km is relatively large for a planetary flyby, the control profile found by InTrance can be used as an initial guess for some local trajectory optimization method with a better local convergence behavior. Alternatively, the neurocontroller parameters found by InTrance can be used as an initial guess for another run of InTrance (with a more demanding final constraint, e.g., 1000 km above the planetary surface). The sail film temperature was limited to $T_{\lim} = 240°\text{C} = 513.15$ K. Figure 6 shows the trajectories and steering profiles for a 0% and a 20% degradation limit. Figure 7a shows the SRD increase and Fig. 7b the variation of the solar distance with time. One can see that the aphelion of the last loop becomes larger with an increasing degradation limit and therefore the final solar photonic assist (SPA), that is, the last close solar approach, occurs later. Figure 8 shows the trip times for various degradation limits and half-life SRDs together with the associated increases.

Fast Transfer to the Heliopause

The third case to estimate the impact of OSSD on solar sail mission performance is a fast solar sail mission to the heliopause. Loosely following the requirements for ESA's interstellar heliopause probe (IHP) study [13,14], the spacecraft should be delivered to the nose of

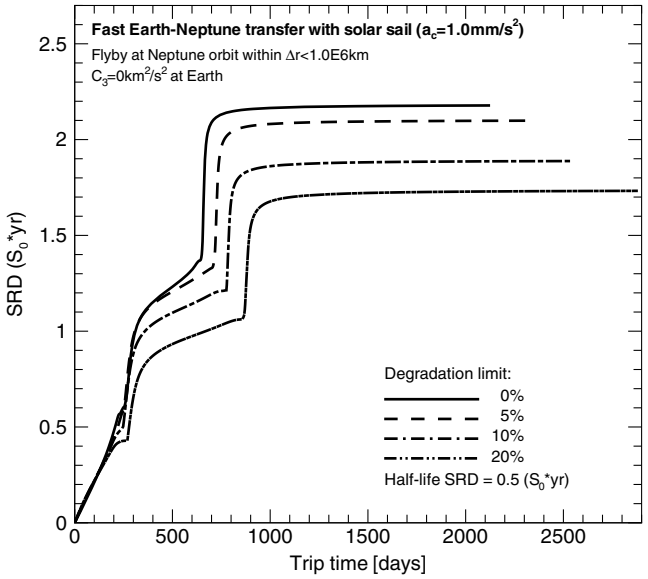

a) Increase of SRD

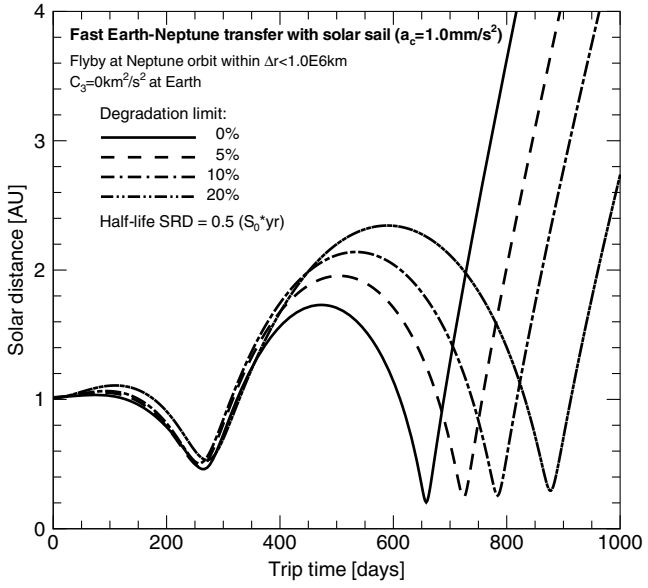

b) Variation of solar distance

Fig. 7 Optimal Neptune transfer for different degradation limits.

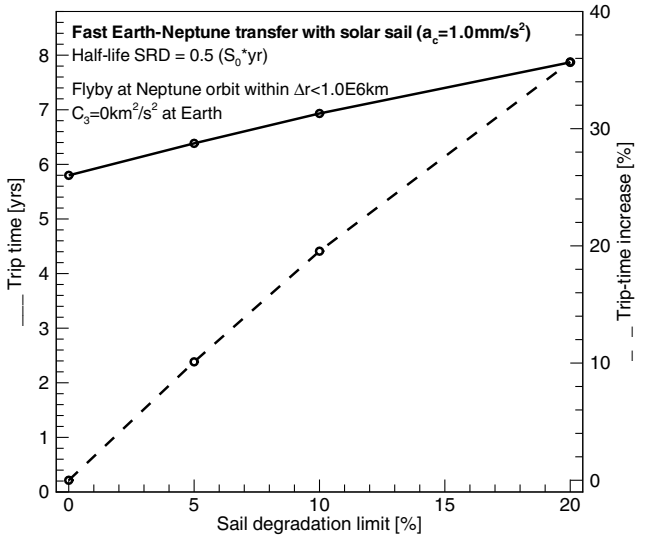

a) Different degradation limits

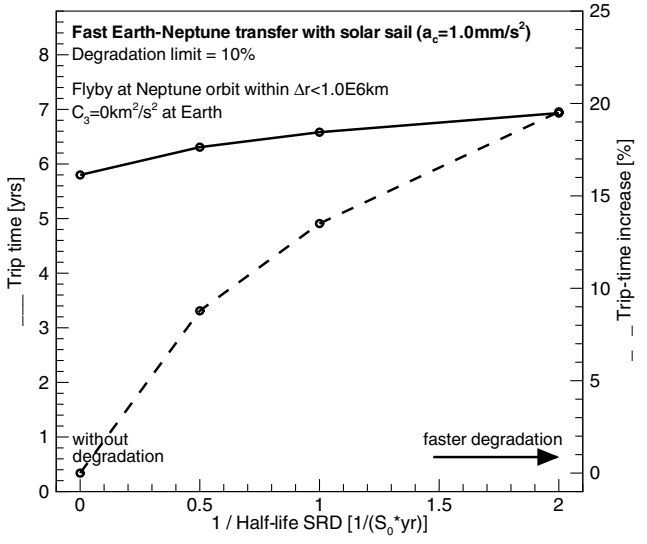

b) Different half-life SRDs

Fig. 8 Trip time and trip-time increase for optimal Neptune transfer.

the heliosphere at a latitude of 7.5° and a longitude of 254.5° (in the ecliptic coordinate frame) at 200 AU from the sun in 25 years. The sail is jettisoned at 5 AU to eliminate any potential interference caused by the solar sail on the local space environment. The trajectories have been calculated using A^nD blending, a method that blends locally optimal control laws [15–17]. Thereby, each control law is prioritized by the consideration of how efficiently it will use the SRP and how far each orbital element is from its target value. For model NPR the trajectories found with A^nD blending and InTrance are very similar [15]. A characteristic acceleration of 1.75 mm/s^2 was selected for this analysis, which gives a zero degradation trip time of 21.74 years. For the trajectories within this section a fixed minimum radius of 0.25 AU, a half-life SRD of $\hat{\Sigma} = 0.5\ (S_0 \cdot \text{yr})$ and a fixed launch date of 03 January 2030 was used. Figure 9a shows the trip time and Fig. 9b shows the trip-time increase for $0 \leq d \leq 0.3$. For $d \leq 0.2$, the trip-time increase is exactly linear. For $d = 0.25$ and 0.3 the trip time does not fit the expected linear relationship as the sail continues to increase the inclination beyond the point where effort would be better spent gaining orbital energy. Figure 9a shows that the radius of aphelion passage increases by over 1 AU as the degradation limit is increased from zero to 30%. Figure 9c shows that the velocity of the spacecraft at sail jettison is decreasing in an approximately linear manner, although the time to sail jettison much more closely matches the shape of the aphelion passage relationship. It is thus notable that given that all these relationships are only *approximately* linear, the trip time to 200 AU is *exactly* linear for $0 \leq d \leq 0.2$. Figure 9d shows the value of the optical coefficients at sail jettison and the total SRD increase with degradation limit. Figure 10a shows the most favorable trajectory plot for each degradation limit. Note that a change in degradation limit for a fixed start epoch significantly changes the final spacecraft azimuth at 200 AU, which would significantly impact mission science objectives. In Fig. 10a it is seen that the SPA occurs at the same physical location independent of the degradation limit as the argument of pericenter is not varied from trajectory to trajectory, although the time of each SPA is seen to vary by as much as $1\frac{1}{4}$ years in Fig. 10b. Figure 10b also shows that for $0 \leq d \leq 0.2$ the inclination has attained its final value significantly before the SPA. At $d = 0.25$ the inclination reaches 7.5° just before the SPA, while at $d = 0.3$ this does not occur until after the SPA. The sail control angles used in each best case trajectory are illustrated in Fig. 11a where it is noted that the maximum pitch angle of each trajectory is similar, while the maximum cone angles decrease in-line with the degradation limit increase. Furthermore, the size of the discontinuity within each control angle profile decreases as d increases. Figure 11b shows the variation of the optical coefficients

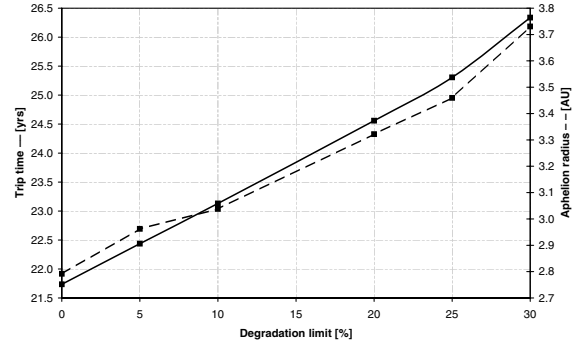

a) Trip time to 200AU and radius of aphelion passage

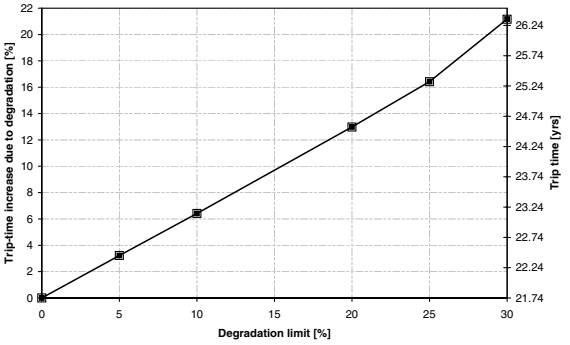

b) Trip-time increase

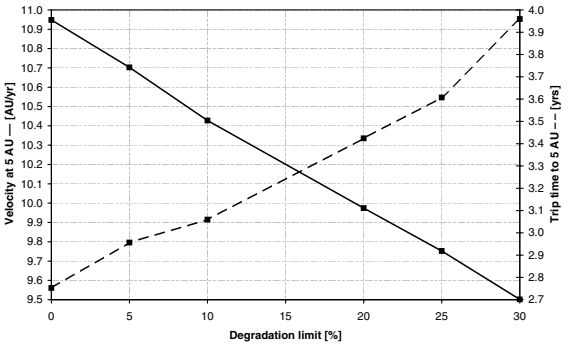

c) Trip time and velocity at 5AU (sail jettison point)

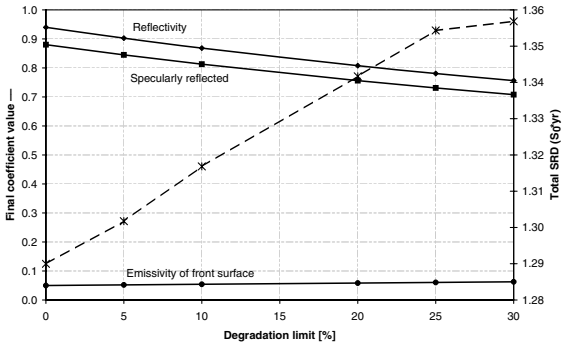

d) Final optical coefficient values and SRD

Fig. 9 Transfer to 200 AU for different degradation limits ($\hat{\Sigma} = 0.5$).

for the trajectories shown in Fig. 10a, where it is seen that the bulk of the degradation occurs during the close solar pass. It is thus logical to assume that multiple close solar passes would have an adverse effect on the quality of the optical surface and should be avoided when designing such trajectories.

Results for Artificial Lagrange-Point Missions

To estimate the impact of OSSD on artificial Lagrange-point missions [18,19], this section will examine this problem for solar sails with different reflection coefficients according to a simplified nonperfectly reflecting solar sail model, which will be described in the next section. First, equilibrium solutions will be obtained for an ideal solar sail. Then, the problem will be revisited for solar sails with nonperfect reflection. Because of the effect that $\boldsymbol{F}_{\mathrm{SRP}}$ is no longer directed along $\boldsymbol{n}$, it will be shown that the volume of space available for artificial Lagrange points is extremely sensitive to the reflection coefficient.

Simplified Model for the Nonperfectly Reflecting Solar Sail

To allow a closed-form solution of the artificial Lagrange-point problem, one must simplify model NPR by assuming specular reflectivity of the sail, $s = 1$, and equal products of the emission coefficient and the non-Lambertian coefficient for the front and back side, $\varepsilon_{\mathrm{fr}} B_{\mathrm{fr}} = \varepsilon_b B_b$. This model will here be denoted as model SNPR (simplified nonperfect reflection). Within model SNPR, the symbol η denotes the reflection coefficient. The SRP force components in the $\mathcal{S}$ frame are in this case

$$F_{\perp} = \quad 2PA\cos\alpha a_1 \cos\alpha \tag{15a}$$

$$F_{\parallel} = -2PA\cos\alpha a_3 \sin\alpha \tag{15b}$$

with

$$a_1 \triangleq \tfrac{1}{2}(1+\eta) \qquad a_3 \triangleq \tfrac{1}{2}(1-\eta) \tag{16}$$

Equilibrium Solutions for the Ideal Sail Model

First, equilibrium solutions for an ideal sail will be derived. The ideal sail will be considered in a frame of reference corotating with the two primary masses m_1 (sun) and m_2 (Earth or other planet) at constant angular velocity $\boldsymbol{\omega}$, as shown in Fig. 12. The sail attitude is defined by the sail normal vector $\boldsymbol{n}$, fixed in the rotating frame of reference. In addition, the ratio of the SRP force to the solar gravitational force exerted on the sail is defined by the sail lightness number β. Because for $m_1 \gg m_2$ both forces have approximately an inverse square variation with solar distance, the sail lightness number is nearly a constant.[††] It can be shown that the sail lightness number is related to the total solar sail mass per unit area σ by $\sigma = 1.53\ \mathrm{g/m^2}/\beta$. Let the unit of mass be chosen such that $\bar{\mu} = G(m_1 + m_2) = 1$. In the system that we now define by $\mu = m_2/(m_1 + m_2)$, the two masses are $\mu_1 = 1 - \mu$ and $\mu_2 = \mu$. The unit of length is chosen such that the constant separation of the two masses is also unity. The vector equation of motion for a solar sail in this rotating frame can be written in standard form as

$$\ddot{\boldsymbol{r}} + 2\boldsymbol{\omega} \times \dot{\boldsymbol{r}} + \nabla U = \boldsymbol{a} \tag{17}$$

with the three-body gravitational potential U and the SRP acceleration $\boldsymbol{a}$ defined by

$$U = -\left[\frac{1}{2}(x^2 + y^2) + \frac{1-\mu}{r_1} + \frac{\mu}{r_2}\right] \tag{18a}$$

$$\boldsymbol{a} = \beta \frac{1-\mu}{r_1^2}(\hat{\boldsymbol{r}}_1 \cdot \boldsymbol{n})^2 \boldsymbol{n} \tag{18b}$$

where the sail position vectors are defined as $\boldsymbol{r}_1 = (x + \mu, y, z)$ and $\boldsymbol{r}_2 = [x - (1-\mu), y, z]$. Equilibrium solutions are now required in the rotating frame so that the first two terms of Eq. (17) vanish. The five classical Lagrange points are then obtained as the solutions of $\nabla U = 0$ with $\hat{\boldsymbol{r}}_1 \cdot \boldsymbol{n} = 0$ (which implies $\boldsymbol{a} = 0$). However, for

[††]Note that the finite size of the solar disk leads to a very small deviation of the SRP from a $1/r_1^2$ law.

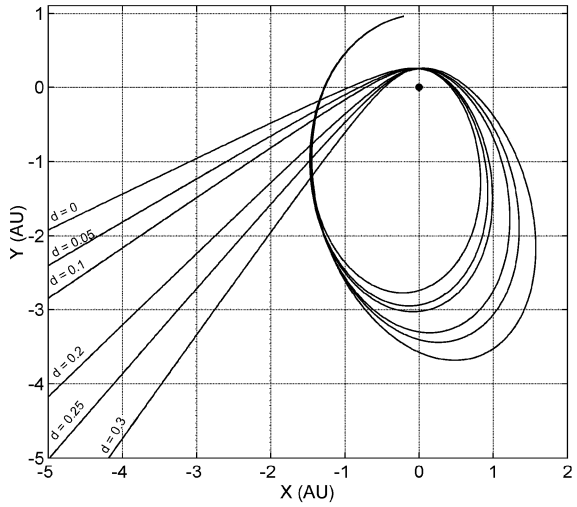

a) Inner solar system trajectories

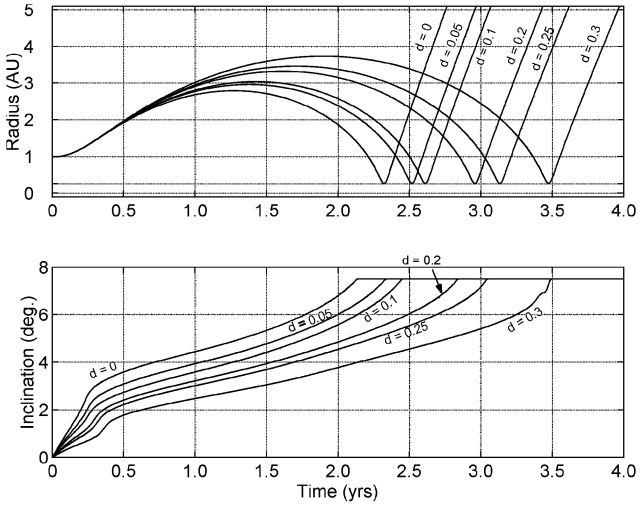

b) Variation of solar distance and inclination

Fig. 10 Transfer to 200 AU for different degradation limits ($\hat{\Sigma} = 0.5$).

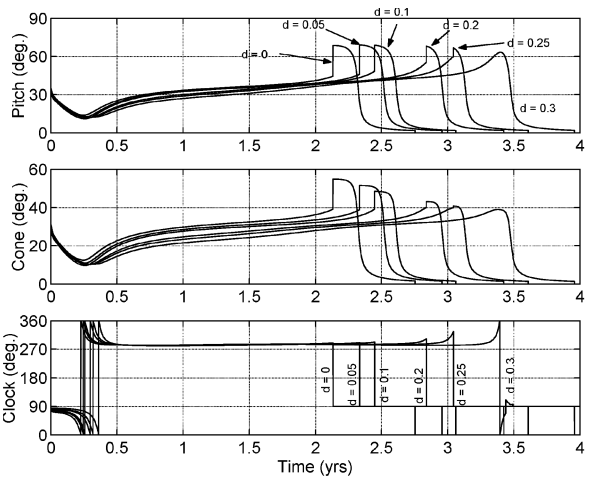

a) Variation of control angles

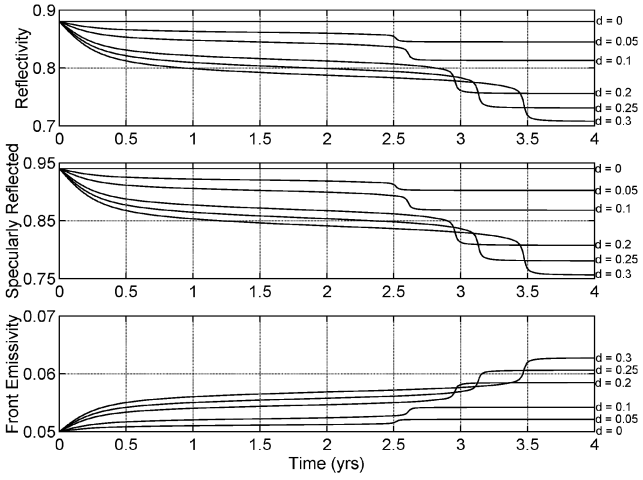

b) Variation of optical coefficients

Fig. 11 Transfer to 200 AU for different degradation limits ($\hat{\Sigma} = 0.5$).

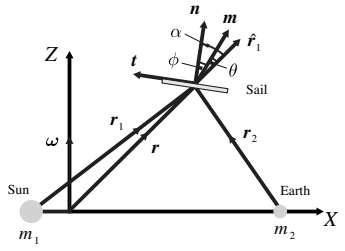

Fig. 12 Sun–Earth restricted circular three-body problem with nonperfectly solar sail.

$\hat{\boldsymbol{r}}_1 \cdot \boldsymbol{n} > 0$, there is an additional acceleration $\boldsymbol{a}$ which is a function of the lightness number β and the attitude $\boldsymbol{n}$ so that new artificial equilibrium solutions may be generated. Because the vector $\boldsymbol{a}$ is oriented in direction $\boldsymbol{n}$, taking the vector product of Eq. (17) with $\boldsymbol{n}$ yields

$$\nabla U \times \boldsymbol{n} = 0 \Rightarrow \boldsymbol{n} = \lambda \nabla U \tag{19}$$

where λ is an arbitrary scalar multiplier. Using $|\boldsymbol{n}| = 1$, λ is identified as $1/|\nabla U|$ so that the required sail attitude is defined by

$$\boldsymbol{n} = \frac{\nabla U}{|\nabla U|} \tag{20}$$

which can be used to obtain the pitch angle α. The required sail lightness number may also be obtained by taking the scalar product of Eq. (17) with $\boldsymbol{n}$. Again, for an equilibrium solution it is found that

$$\beta = \frac{r_1^2}{1-\mu} \frac{\nabla U \cdot \boldsymbol{n}}{(\hat{\boldsymbol{r}}_1 \cdot \boldsymbol{n})^2} \tag{21}$$

Because the sail lightness number and attitude can be selected, the set of five classical Lagrange points is replaced by an infinite set of artificially generated equilibrium solutions. The regions in which these new solutions may exist are defined by the constraint $\hat{\boldsymbol{r}}_1 \cdot \nabla U \geq 0$ with a boundary surface defined by the equality sign. This constraint can be physically explained by observing that the SRP acceleration vector $\boldsymbol{a}$, and so the sail normal vector $\boldsymbol{n}$, can never be directed sunward. The boundary surface has two topologically disconnected surfaces S_1 and S_2 which define the region of existence of equilibrium solutions near m_2. The classical equilibrium solutions lie on either S_1 or S_2 because they are the solutions of $\nabla U = 0$. Surfaces of the constant sail lightness number generated from Eq. (21) for the Earth–sun system are shown in Fig. 13a. In general, the surfaces of the constant sail lightness number approach these boundaries asymptotically with $\beta \to \infty$ when $\hat{\boldsymbol{r}}_1 \cdot \boldsymbol{n} \to 0$ as is clear from Eq. (21). It can be seen that as the sail lightness number increases, larger volumes of space are accessible for artificial equilibrium points.

Equilibrium Solutions for the Nonperfectly Reflecting Solar Sail with Optical Degradation

When model SNPR is used instead of model IR, the SRP acceleration acts in the direction of $\boldsymbol{m}$ and may be written as the sum

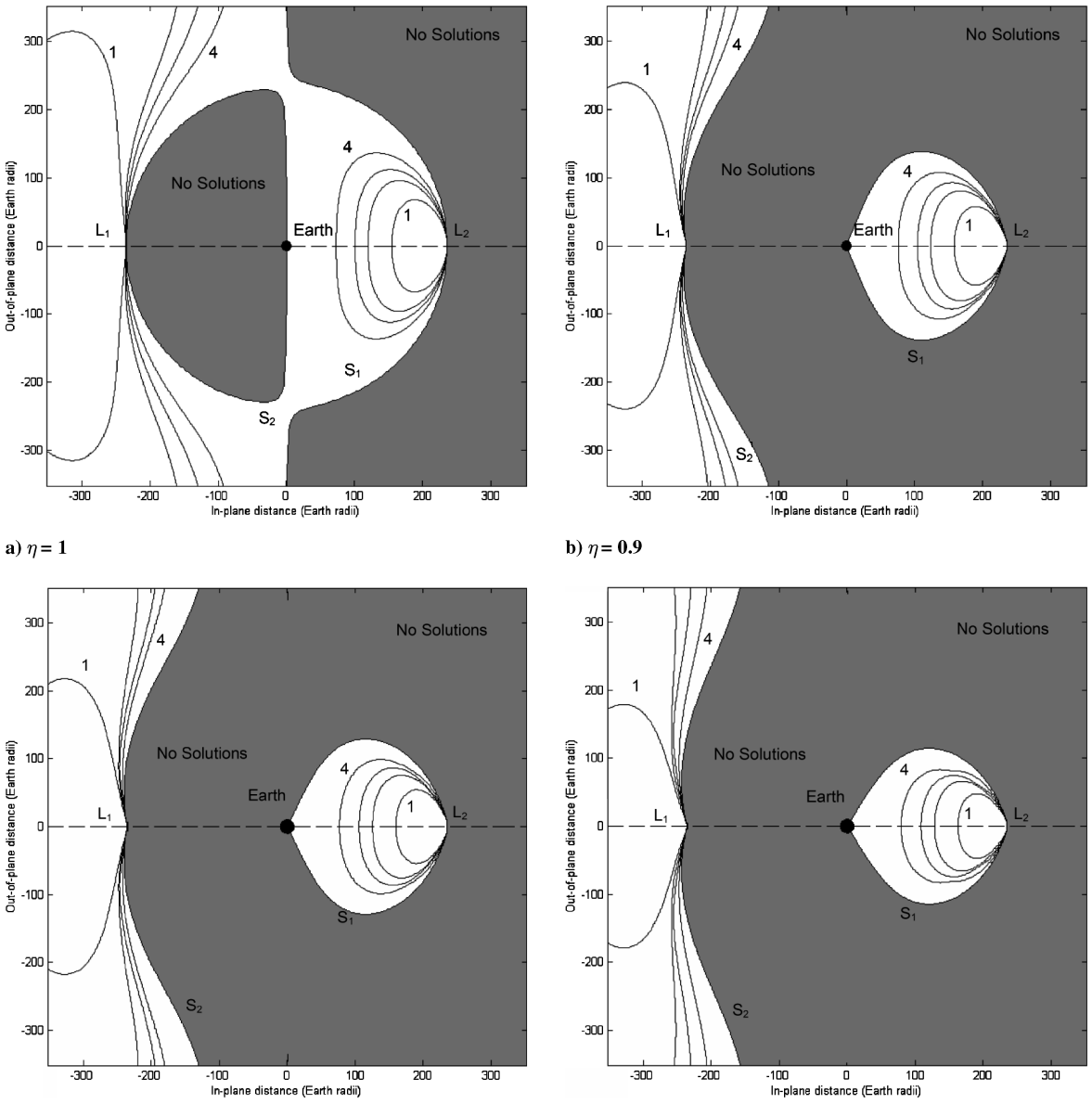

a) $\eta = 1$ **b)** $\eta = 0.9$

c) $\eta = 0.8$ **d)** $\eta = 0.7$

Fig. 13 Contours of sail loading σ in the x–z plane: [1] 30 [2] 15 [3] 10 [4] 5 (in g/m^2).

of components normal to the sail surface (along $\boldsymbol{n}$) and transverse to the sail surface (along $\boldsymbol{t}$)

$$a\boldsymbol{m} = \frac{1}{2}\beta\frac{1-\mu}{r_1^2}(1+\eta)(\hat{\boldsymbol{r}}_1\cdot\boldsymbol{n})^2\boldsymbol{n} + \frac{1}{2}\beta\frac{1-\mu}{r_1^2}(1-\eta)(\hat{\boldsymbol{r}}_1\cdot\boldsymbol{n})(\hat{\boldsymbol{r}}_1\cdot\boldsymbol{t})\boldsymbol{t} \tag{22}$$

where $(\hat{\boldsymbol{r}}_1\cdot\boldsymbol{n}) = \cos\alpha$ and $(\hat{\boldsymbol{r}}_1\cdot\boldsymbol{t}) = \sin\alpha$. The analysis presented in the previous section will now be repeated using the sail force model defined by Eq. (22) so that the equation of motion can now be written as

$$\ddot{\boldsymbol{r}} + 2\boldsymbol{\omega}\times\dot{\boldsymbol{r}} + \nabla U = a\boldsymbol{m} \tag{23}$$

For an equilibrium solution to exist, the first two terms of Eq. (23) will again vanish so that the sail attitude must be chosen as

$$\boldsymbol{m} = \frac{\nabla U}{|\nabla U|} \tag{24}$$

The unit vector $\boldsymbol{m}$ can now be defined by the cone angle θ between $\hat{\boldsymbol{r}}_1$ and $\boldsymbol{m}$ as

$$\tan\theta = \frac{|\hat{\boldsymbol{r}}_1\times\nabla U|}{\hat{\boldsymbol{r}}_1\cdot\nabla U} \tag{25}$$

In addition, using Eq. (22), the centerline angle can be obtained from the ratio of the transverse and normal accelerations as

$$\tan\phi = \frac{1-\eta}{1+\eta}\tan\alpha \tag{26}$$

where the pitch angle $\alpha = \theta + \phi$. Noting that $\boldsymbol{n}\cdot\boldsymbol{t} = 0$ and taking a scalar product of Eq. (23) with the unit vector $\boldsymbol{n}$ gives the required sail lightness number as

$$\beta = \frac{2r_1^2}{1-\mu}\frac{\nabla U\cdot\boldsymbol{n}}{(1+\eta)(\hat{\boldsymbol{r}}_1\cdot\boldsymbol{n})^2} \tag{27}$$

The centerline angle can be obtained explicitly by again noting that $\alpha = \theta + \phi$. Then, after some reduction, Eq. (26) yields the centerline angle directly from the cone angle as

$$\tan\phi = \frac{\eta}{(1+\eta)\tan\theta}\left[1 - \sqrt{1 - \frac{1-\eta^2}{\eta^2}\tan^2\theta}\right] \tag{28}$$

Last, using Eq. (27) it is found that the required sail lightness number may be obtained in terms of the lightness number for an ideal solar sail $\tilde{\beta}$ as

$$\beta = \frac{2}{1+\eta}\frac{\sqrt{1+\tan^2\phi}}{(1-\tan\theta\tan\phi)^2}\tilde{\beta} \tag{29}$$

where $\tilde{\beta}$ is defined by Eq. (21). Therefore, using Eqs. (25), (28), and (29) the sail orientation and sail lightness number required for an artificial equilibrium solution can be obtained. The effect of a nonideal solar sail and OSSD is shown in Fig. 13 for $\eta = 0.9, 0.8$, and 0.7. First, it can be seen that the volume of space available for equilibrium solutions about L2 is significantly reduced. This is due to the centerline angle which limits the direction in which the SRP force vector can be directed. For solutions near L1 the main effect of the nonideal sail is to displace the equilibrium solutions toward the Earth. This is due to the reduction in the SRP force magnitude rather than the centerline angle. In general, we can state that equilibrium solutions sunward of L1 are not greatly effected by OSSD while equilibrium solutions about L2 are severely restricted.

Conclusions

Using a parametric model that includes the optical degradation of the sail film due to the erosive effects of the space environment, the impact of different potential degradation behaviors on solar sail mission performance has been estimated for various example missions. Our results show that optical solar sail degradation has in most cases a considerable effect on both the trip time and the optimal steering profile of interplanetary transfer missions. For specific launch dates, especially those that are optimal without degradation, this effect can be tremendous. For artificial Lagrange-point missions, the equilibrium solutions sunward of L1 are, in general, not greatly affected by optical solar sail degradation, while equilibrium solutions about L2 are severely restricted.

Having demonstrated the *potential* effects of optical solar sail degradation on future missions, an in-depth research on the *real* degradation behavior is now advisable. In fact, the degradation behavior of the sail's propulsive capability in a real space environment is still, to a great extent, unknown. To narrow down the ranges of the parameters of the degradation model, further laboratory testing has to be performed. Additionally, before a mission that relies on solar sail propulsion is flown, the candidate solar sail films have to be tested in the relevant space environment. For doing that, some near-term missions currently studied in the United States and in Europe would be an ideal opportunity.

Acknowledgments

The authors would like to thank the members of the "Solar Sail Degradation Model Working Group" (SSDMWG) for supporting their work: Wolfgang Seboldt (DLR, Cologne, Germany), Leonel Rios-Reyes and Daniel J. Scheeres (University of Michigan, Ann Arbor, Michigan), Bong Wie (Arizona State University, Tempe, Arizona), Marianne Görlich and Franz Lura (DLR, Berlin, Germany), Benjamin Diedrich (NOAA, Silver Spring, Maryland), Volodymyr Baturkin (National Technical University of Ukraine, Kiev, Ukraine), Victoria L. Coverstone (University of Illinois at Urbana–Champaign, Urbana, Illinois), Manfred Leipold (Kayser-Threde GmbH, Munich, Germany), and Gregory P. Garbe (NASA Marshal Space Flight Center, Huntsville, Alabama).

References

[1] McInnes, C., "Delivering Fast and Capable Missions to the Outer Solar System," *Advances in Space Research*, Vol. 34, No. 1, 2004, pp. 184–191.

[2] Mengali, G., and Quarta, A., "Time-Optimal Three-Dimensional Trajectories for Solar Photon Thruster Spacecraft," *Journal of Spacecraft and Rockets*, Vol. 42, No. 2, 2005, pp. 379–381.

[3] Dachwald, B., "Minimum Transfer Times for Nonperfectly Reflecting Solar Sailcraft," *Journal of Spacecraft and Rockets*, Vol. 41, No. 4, 2004, pp. 693–695.

[4] Wright, J., *Space Sailing*, Gordon and Breach Science Publishers, Philadelphia, 1992, pp. 227–233.

[5] Forward, R., "Grey Solar Sails," *Journal of the Astronautical Sciences*, Vol. 38, No. 2, 1990, pp. 161–185.

[6] McInnes, C., *Solar Sailing. Technology, Dynamics and Mission Applications*, Springer–Praxis Series in Space Science and Technology, Springer–Praxis, Berlin, 1999, pp. 46–53.

[7] Rios-Reyes, L., and Scheeres, D., "Generalized Model for Solar Sails," *Journal of Spacecraft and Rockets*, Vol. 42, No. 1, 2005, pp. 182–185.

[8] Lura, F., Hagelschuer, D., Glotov, A., and Tschaly, Y., "Experiments in the Test Facility KOBE for the Investigation of Degradation Effects on Thin Foil Samples for a Solar Sail Mission Concerning the Simultaneous Influence of Space Environment Properties," *Proceedings of the 22nd Space Simulation Conference*, Oct. 2002.

[9] Edwards, D., Hubbs, W., Stanaland, T., Hollerman, A., and Altstatt, R., "Characterization of Space Environmental Effects on Candidate Solar Sail Material," *Photonics for Space Environments VIII: Proceedings of SPIE*, edited by E. Taylor, Vol. 4823, (SPIE–International Society for Optical Engineering, Bellingham, WA, 2002, pp. 67–74.

[10] Dachwald, B., Mengali, G., Quarta, A., and Macdonald, M., "Parametric Model and Optimal Control of Solar Sails with Optical Degradation," *Journal of Guidance, Control, and Dynamics*, Vol. 29, No. 5, 2006, pp. 1170–1178.

[11] Gill, P., Murray, W., and Saunders, M., "User's Guide for SNOPT 5.3: A FORTRAN Package for Large-Scale Nonlinear Programming," Tech. Rept., Stanford University, 1998.

[12] Dachwald, B., "Low-Thrust Trajectory Optimization and Interplanetary Mission Analysis Using Evolutionary Neurocontrol," Ph.D. Thesis, Universität der Bundeswehr München, Fakultät für Luft-und Raumfahrttechnik, Neubiberg, Germany, 2004.

[13] Lyngvi, A., Falkner, P., Renton, D., v.d. Berg, M., and Peacock, A., "Technology Reference Studies," IAC Paper 04-U.1.06, Oct. 2004.

[14] Lyngvi, A., Falkner, P., Kemble, S., Leipold, M., and Peacock, A., "The Interstellar Heliopause Probe," IAC Paper 04-Q.2.a.06, Oct. 2004.

[15] Macdonald, M., McInnes, C., and Dachwald, B., "Heliocentric Solar Sail Orbit Transfers with Locally Optimal Control Laws," *Journal of Spacecraft and Rockets*, Vol. 44, No. 1, 2007, pp. 273–276.

[16] Macdonald, M., and McInnes, C., "Realistic Earth Escape Strategies for Solar Sailing," *Journal of Guidance, Control, and Dynamics*, Vol. 28, No. 2, 2005, pp. 315–323.

[17] Macdonald, M., and McInnes, C., "Analytical Control Laws for Planet-Centred Solar Sailing," *Journal of Guidance, Control, and Dynamics*, Vol. 28, No. 5, 2005, pp. 1038–1048.

[18] McInnes, C. R., McDonald, A. J. C., Simmons, J. F. L., and MacDonald, E. W., "Solar Sail Parking in Restricted Three-Body Systems," *Journal of Guidance, Control, and Dynamics*, Vol. 17, No. 2, 1994, pp. 399–406.

[19] McInnes, C., "Artificial Lagrange Points for a Non-Perfect Solar Sail," *Journal of Guidance, Control, and Dynamics*, Vol. 22, No. 1, 1999, pp. 185–187.

D. Edwards
Associate Editor